Nucleation Kinetics of the Potassium Sulfate-Water System

ALAN D. RANDOLPH and MICHAEL D. CISE

Department of Chemical Engineering
University of Arizona, Tucson, Arizona 85721

Secondary nucleation in the potassium sulfate-water system occurs by micro-attrition processes over the entire 1.3-26 μ size range of this study. Experimental nucleation rates were correlated with power-law kinetics expressions in terms of supersaturation, the fourth moment of the parent seed-crystal distribution, and stirring rate. Such kinetics expressions are similar to those used to correlate MSMPR data; however, the secondary nucleation rates of this paper are two orders of magnitude greater than those reported in previous MSMPR studies of the same system. An upper bound on growth rate of these nuclei was calculated based on a population balance analysis; maximum growth rates of these nuclei was markedly size-dependent in the 1.3-26 micron size range of measurement, decreasing with decreasing size. The apparent discrepancy between these nucleation rates and MSMPR values can be explained by nuclei washout during the low growth rate period. Anomalous MSMPR kinetics (low or even negative supersaturation power-law dependence) can be explained by this growth phenomenon.

In a companion paper (3) the authors describe an apparatus for the direct quantitative measurement of secondary nucleation in a realistic mixed-magma environment. Extensive data on the potassium sulfate system were presented which clearly indicated that potassium sulfate nucleates at these low supersaturations by collision breeding or micro attrition mechanisms. The present paper analyzes these data by several quantitative techniques and presents correlations describing secondary nucleation rate in terms of variables characterizing the secondary environment.

Crystal nucleation has been shown to occur by at least three separate mechanisms: homogeneous, heterogeneous, and secondary. Homogeneous nucleation occurs from clear solutions by molecular driving forces (supersaturation) while heterogeneous nucleation is stimulated by the presence of foreign substrates. On the other hand, secondary nucleation occurs due to the presence of crystals of the solute phase and commonly occurs at supersaturations lower than required for homogeneous or heterogeneous nucleation. Recent work by Clontz and McCabe (4) indicates the likelihood that secondary nucleation mechanisms predominate in continuous mixed-magma crystallizers. In their work, nucleation was made to occur in slightly supersaturated solutions when crystals were contacted with low energy impacts with glass or metal rods or with other crystals.

Mason and Strictland-Constable (8) identified three types of secondary nucleation:

1. Spurious dusting from the surface of dry seed crystals,
2. Breaking-off from seed crystals of dendritic growth formed at high supersaturations, and
3. Micro-attrition (collision breeding) from large seeds in the mixed-magma due to crystal-crystal, crystal-vessel, and crystal-impeller collisions.

Secondary nucleation of the latter type was identified as the nucleating mechanism for the potassium sulfate system in the companion paper (3); quantitative empirical kinetics correlations for these data are presented here.

Previously, nucleation kinetics for crystallizers of the continuous backmixed type have been obtained from analysis of steady state CSD's from the MSMPR (Mixed Suspension, Mixed Product Removal) crystallizer (*1, 7, 11, 13*). Interpretation of such data was made with the well-known exponential population distribution

$$n(L) = \frac{B^0}{G} \exp\{-L/G\tau\} \qquad (1)$$

Equation (1) assumes the linear growth rate G to be size-independent and gives the apparent net nucleation rate B^0. Typically, values for nucleation rate are measured under different experimental conditions and power-law kinetics correlations of the type

$$B^0 = k_N(T, RPM)\, s^i M_T^j \quad \text{(Class I system)} \qquad (2)$$

or

$$B^0 = k_N(T, RPM)\, G^i M_T^j \quad \text{(Class II system)} \qquad (2a)$$

are assembled from the data. Even though such kinetic expression do not elucidate the mechanisms giving rise to secondary nucleation, they have been found a useful means of correlating data for prediction of CSD.

Two aspects of MSMPR kinetics will be mentioned here and discussed later in light of data from the present study. First, B^0 values are calculated by extrapolating the measured CSD of macro-sized crystals back to zero size to obtain the apparent rate of nucleation. Second, processes of birth, growth, and washout at very small size are not measured; values of B^0 calculated are thus in fact *net* apparent nucleation rates which eventually populate the macro size ranges under the conditions of MSMPR operation. If these conditions are not far removed from commercial practice, conclusions can be drawn concerning the apparent kinetics of the system and such data are often quite valuable in predicting large-scale CSD behavior.

The present study measures experimental population densities in the 1.3-26 micron size range; sizes small enough that direct observations of secondary nucleation could be made. Growth, birth, and washout dynamics were grossly different at these small sizes than for macro-sized crystals. Secondary nucleation was of a greater magnitude than, but could be correlated with power-model kinetics similar to, MSMPR nucleation data.

M. D. Cise is with Eli Lilly and Company, Indianapolis, Indiana.

EXPERIMENT

Crystal population densities of the potassium sulfate-water system were measured in the 1.3-26 micron size range in a modified mixed discharge crystallizer using a multi-channel high speed automatic Coulter particle counter. The equipment and experimental data are described in detail elsewhere (*2, 3, 12*). The essential feature of the crystallizer was a fine-mesh stainless steel retaining screen which permitted mixed removal of the fine seed distribution with total retention of macro-sized seed crystals. The fines distribution in the 1.3-26 micron size range was sampled in the discharge from the screen with a modified on-line Coulter sampling cell. Total retention of seed crystals permitted study of secondary nucleation in the presence of arbitrary seed distributions and supersaturations with small retention times and hence fast system response. Unfortunately, total retention of the seed crystals, with their resultant increase in size and mass, created a slowly changing secondary nucleation environment; data were analyzed using the dynamic form of the population balance.

Figure 1 from (*3*) shows population data of this study. Note in Figure 1 the ever increasing particle counts as time progresses due to total retention and growth of the seed crystals. Typically, supersaturation decreased as the seed bed grew in mass; thus, size of the seed crystals outweighs supersaturation in stimulating secondary nuclei. Secondary nucleation increased dramatically with increases in stirrer RPM, implying that the size channels are populated at least in part by direct birth as that size. Crystal populations increased with supersaturation but this effect was compounded with a more rapid growth to larger sizes of the retained seeds. Potassium sulfate seed crystals of multi-crystal habit generated larger particle counts than seed of single-crystal form under approximately equal conditions of seed mass, size, supersaturation, and agitation. Crystallizer temperature was varied while holding feed saturation constant; again, such changes were compounded with the independent effects of supersaturation and seed size and mass.

In the present paper, raw population counts as a function of time and particle size were quantitatively analyzed to obtain estimates of secondary nucleation rate. Nucleation rate data were then correlated with power-law kinetic expressions not unlike those previously used to express MSMPR data.

ANALYSIS OF DATA

The starting point in the analysis of these data is the general population balance (*10*) given as

$$\frac{\partial n}{\partial t} + \frac{\partial (Gn)}{\partial L} + n\frac{d(\ln V)}{dt} = \sum_i \frac{n_i \vec{Q}_i}{V} + B(L) - D(L) \qquad (3)$$

The complexity of this equation can be reduced by considering that the slurry volume V was maintained essentially constant throughout any one run, that the system was well mixed with mixed withdrawal in the size range studied, and that background noise counts taken prior to seeding indicated that the feed stream was free of fine crystals. The death distribution function of Equation (3) was neglected as negligible crystal fracture in the 1.3-26 micron size range occurred. However, the birth distribution term was retained as an expression of the formation of nuclei by micro-attrition (collision breeding) phenomenon originating from the larger seed crystals. Thus, Equation (3) becomes

$$\frac{\partial n}{\partial t} + \frac{\partial (Gn)}{\partial L} = -\frac{n}{\tau} + B(L) \qquad (4)$$

Solving Equation (4) for linear crystal growth rate gives

$$G(L,t) = -\frac{\left[\dfrac{\partial(\ln n)}{\partial t} + \dfrac{1}{\tau} + \dfrac{\partial G}{\partial L} - \dfrac{B(L)}{n}\right]}{\dfrac{\partial(\ln n)}{\partial L}} \qquad (5)$$

Alternatively, Equation (4) can be solved for the birth function $B(L)$. Thus

$$B(L) = n\frac{\partial(\ln n)}{\partial t} + \frac{\partial(Gn)}{\partial L} + \frac{n}{\tau} \qquad (6)$$

Equations (4) to (6) contain two unknown functions of particle size, namely size-dependent growth rate $G(L)$ and the birth distribution function $B(L)$. Thus, it is patently impossible to uniquely specify both size-dependent functions $B(L)$ and $G(L)$ using only the single size dependent measurement $n(L)$, without further simplifying assumptions or independent measurements. This dilemma was faced by utilizing two different limiting assumptions which, however, introduce a degree of arbitrariness in the definition of nucleation rates calculated from raw population counts. These two limiting assumptions are as follows:

Method 1

Birth at a size is assumed zero. Thus $B(L) = 0$ and $G(L)$ is calculated from experimental $n(L)$ measurements using Equation (5). All size ranges are assumed populated by convective growth from a lower size. Size-dependent number flux is given as the product $n(L)\ G(L)$ and nucleation rate is defined as the number flux at some arbitrary nuclei size L_0. Thus

$$B_1^0 = G(L_0)\ n(L_0) \qquad (7)$$

For $G \neq G(L)$, $n(L)$ given by an exponential in L and $L_0 = 0$, this technique leads to the classical MSMPR definition of nucleation rate.

Method 2

Population changes due to convective number flux are suppressed. Thus $\dfrac{\partial(nG)}{\partial L} = 0$ and the birth function, balanced by particle washout and accumulation, is given by Equation (6) as

$$B(L) = n\left[\frac{\partial(\ln n)}{\partial t} + \frac{1}{\tau}\right] \qquad (8)$$

Nucleation rate is then taken as the sum of all particle births, namely

$$B_2^0 = \int_0^\infty B(L)\, dL \qquad (9)$$

Even if nucleation occurs over a size range and is de-

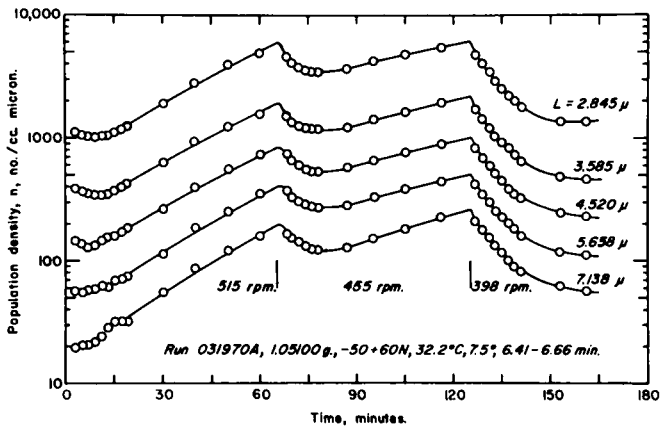

Fig. 1. Effect of stirring rate increase on population densities (*3*).

scribed by a birth function $B(L)$, convective growth of the secondary nuclei must occur in order to populate the larger size ranges. However, if the growth rate of secondary nuclei is small and the crystallizer is operated with a short retention time (both true for this study) then particle washout and accumulation approximately balance birth and Equation (9) is a good representation of nucleation rate.

Both Methods 1 and 2 were used to quantitatively reduce the population counts of this study to nucleation and growth rate B_1^0 and $G(L)$ and nucleation rate B_2^0, respectively. In addition, growth rates of the macro-sized seed crystals were calculated from photomicrographs taken during the run.

As suggested by previous nucleation correlations, these data were correlated with power-law kinetics of the form

$$B^0 = k_N \exp\{k_1/T\}\, s^{k_2}\, m_j^{k_3}\, (Re_s)^{k_4} \qquad (10)$$

where the stirring Reynolds number $Re_s = R_s d_i^2 \rho/\mu$ was used to represent changes in agitation level caused by different stirrer RPM's.

The growth kinetics model of the macro-sized seed crystals considered temperature, supersaturation, size-dependency, and agitation rate. The exponential temperature term is considered to be an Arrhenius expression for the surface reaction step of crystal growth, tantamount to neglecting solute diffusion in the overall growth process. Ishii (6) and Mullin and Gaska (9) have employed this exponential form of temperature-dependence in their studies of the potassium sulfate system.

Power model terms for the supersaturation and size dependence were used. Agitation effects were correlated in terms of an exponential of the stirring rate exp $(k_4 R_s)$. Thus, the general growth kinetics model used for fitting growth rate data of the seed crystals was of the form

$$G_p = k_g \exp(k_1/T)\, s^{k_2}\, (L)^{k_3} \exp(k_4 R_s) \qquad (11)$$

Growth rates of the fine-crystal distribution in the 1.3-26 micron size range were calculated from Equation (5) using an iterative technique to obtain $\partial G/\partial L$ and by suppressing the $B(L)$ term; such values represent a maximum estimate of the true nuclei growth rate. The size-dependence of the fine-crystal growth rates was found to be correlated with an equation of the form

$$G(L) = G_\infty \exp\{-k/L^{1/2}\} \qquad (12)$$

The parameter G_∞, physically representing the extrapolated growth rate to infinite size, was then correlated with an equation of the form

$$G_\infty = k_g \exp\{k_1/T\}\, s^{k_2} \qquad (13)$$

The parameter k_1 did not correlate with operating conditions nor did G_∞ correlate with agitation rate.

DATA TREATMENT

A complete description of all analytical techniques for data reduction is given by Cise (2). Simply, treatment of the population data of this study involved fitting ln n vs. L data with polynomials of order one through four. These polynomial relationships were differentiated to obtain slope values suitable for use in Equations (5) and (6).

The effectiveness of a correlating model was judged by the value of the square of the correlation coefficient obtained from a library multiple linear regression computer program. The empirical correlation equation forms, Equations (10) to (13), were linearized by data fitting in log-space.

FINE-CRYSTAL GROWTH DATA CORRELATION

Linear growth rates in the 1.3-26 micron size range were determined using Equation (5) with the birth term $B(L)$ taken as zero, that is, the assumptions of Method 1 data analysis technique. These values represent an upper bound on growth rate. As $B(L)$ surely approaches zero at the upper size range of measurement it can be asserted that growth rate is at least as size-dependent as calculated by Equation (5). Growth rates of the smaller sizes are undoubtedly lower than calculated by this technique. Growth rate data calculated using Equation (5) from 38 runs were fitted with Equation (12) and the values of G_∞ were correlated with Equation (13). A similar model which included the stirring rate term was tested with these data; the statistics indicated that stirring rate had an indiscernible effect on G_∞. These data correlated as

$$G_\infty = \exp(13.269) \exp(-4390/T)\, s^{0.987} \qquad (14)$$

with $r^2 = 0.425$ (log plane), indicating a poor level of correlation with operating conditions. Values of k were in the range 2.4 to 5.5 but did not correlate with operating conditions; however, each individual run correlated well with the size dependence shown in Equation (12), (typically, $r^2 > 0.95$).

Figure 2 from (3) shows the extreme size-dependence of growth rates in the size range studied for typical runs of this study. The higher growth rates shown in Figure 2 were obtained under conditions of higher supersaturation. It should be emphasized that the growth rates calculated represent only an upper asymptotic bound corresponding to the assumption $B(L) = 0$. Actual growth rates are, in fact, lower than the values shown in Figure 2.

SEED-CRYSTAL GROWTH RATE CORRELATION

Average growth rates of seed crystals were obtained from photographs of the initial and product seed distributions by dividing the increase in averaged particle equivalent spherical diameter by the total time spent within the crystallizer. Mean supersaturations were evaluated by graphical integration of the concentration histories for each run.

Averaged seed growth rates for 34 runs were obtained using various fractions of rhombic seeds at various temperatures, supersaturations, and stirring rates. These data were correlated by the kinetics model of Equation (11). Correlation statistics showed that stirring rate did not have an appreciable effect on the fit of the data; thus the

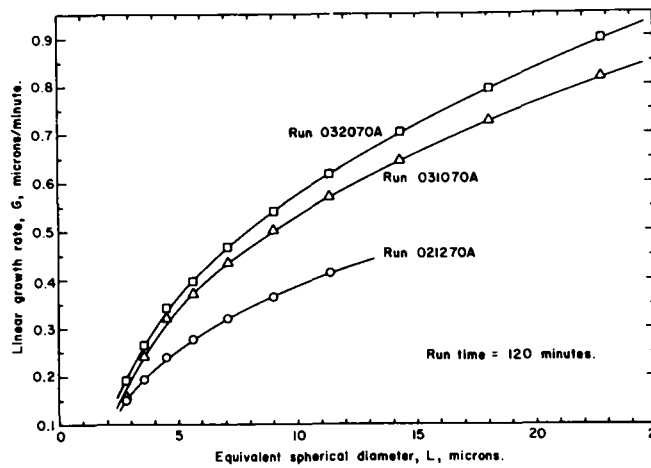

Fig. 2. Size-dependent growth rates calculated assuming $B(L) = 0$.

stirring rate term was deleted. The final form and constants of the correlation yielded the relation

$$G_p = \exp(38.755) \exp(-10725/T)\, s^{1.930} \exp(-181/L^{1/2}) \quad (15)$$

with $r^2 = 0.954$ (log plane).

The functionality of supersaturation is plotted against supersaturation in Figure 3 for the evaluated models of Equations (14) and (15), that is, for the fine-crystal and seed-crystal distributions. Experimental values of $F(s)$ for the seed-crystal growth rates are plotted to show their agreement with the predicted values. Although the form of the temperature, supersaturation, and size dependencies of growth rate for fine-crystals and seeds were identical, the specific correlating constants were grossly different, and fine-crystal growth rates predicted by Equations (12) and (14) do not extrapolate to the values measured for the seeds.

Growth rate for the seed crystals (630-1430 microns) is approximately a function of s^2. Mullin and Gaska (9) reported that potassium sulfate crystals in the 250-2500 micron mean size range grew at a rate proportional to the square of the supersaturation. Rosen and Hulburt (*14*) reported an identical functionality for the 60-2000 micron size range. Ishii (*6*), on the other hand, reported a first-order supersaturation relationship for potassium sulfate corresponding to the correlation obtained for G_x values.

The activation energy for the growth rate of seeds is 21.3 kcal/g.-mole. Mullin and Gaska (9) reported a value of 4.3 kcal/g.-mole for their study of potassium sulfate over a 10° to 50°C temperature range. Ishii (*6*) reported an activation energy value of 17.2 kcal/g.-mole for the same temperature range.

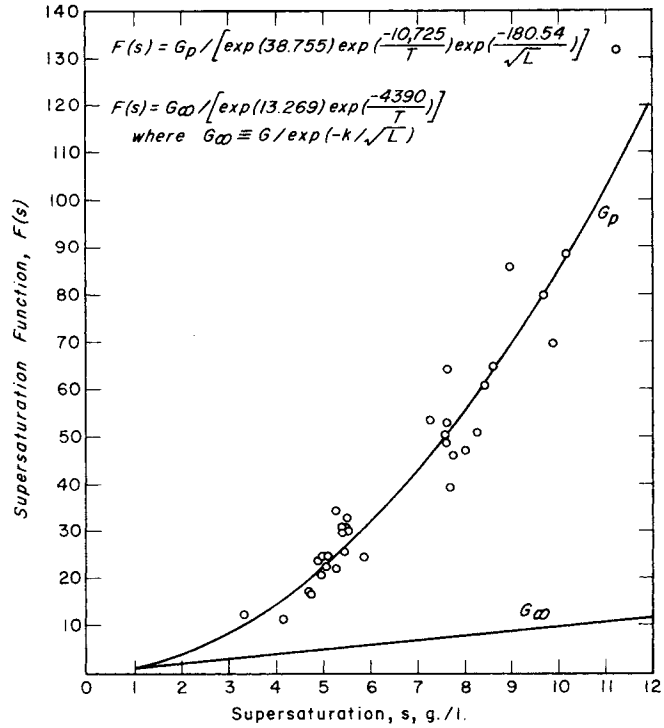

Fig. 3. Comparison of supersaturation functionalities for growth rate models of fine-crystal and seed-crystal distributions. Photographically-determined growth rate data sets of seed crystals are represented by the circles.

MAXIMUM PARTICLE FLUX CORRELATION (METHOD 1)

Nucleation rates were calculated by the two methods of analysis of the population density data described previously, namely the calculation of the apparent maximum particle flux by extrapolation of the product of growth rate times nuclei density, both given by analytical empirical expressions, to a size close to zero, and the use of a birth distribution function to account for the appearance of nuclei at very small sizes while suppressing particle convection due to growth. The particle flux technique (Method 1) of calculating nucleation rate has been reported in previous work with MSMPR crystallizers (*4, 5,* 7). Nucleation flux at size zero, as defined by Equation (7), is conventionally expressed as

$$B_1^0 = G(0) \cdot n(0) \quad (16)$$

In this study $G(0)$ as expressed by Equation (12) has the value of zero. The value for $n(0)$ is usually taken as the intercept on a semi-log plot of the population density versus size. Examination of typical distributions from this study indicates the impossibility of extrapolating such data. Since B_1^0 clearly goes to zero in the case where growth rate is given by Equation (12), a maximum apparent flux was calculated from analytical empirical expressions for $n(L)$ and $G(L)$ and was used as the definition of particle generation flux B_1^0. However, nucleation rates calculated by this technique (Method 1) did not correlate well with operational conditions (typical r^2 correlation coefficients in the range 0.45 to 0.5) and thus Method 2 (birth distribution technique) was used as a better quantitative definition of nucleation rate for the data of this study. However, an attempt to correlate B_1^0 data to operating conditions was made, with the results shown below in the kinetic correlation Equations (17) to (19). Rhombic seeds were used in every case with a common stirring rate of 515 rev./min., using a 4-bladed impeller. Thus, stirring rate was omitted as a factor in the correlations. Correlations were obtained for the third, fourth, and fifth moments of the seed distribution. The resultant relationships are

$$B_1^0 = \exp(-35.555) \exp(+8536/T)\, s^{-0.786}\, m_3^{0.849} \quad (17)$$

for the third moment with $r^2 = 0.477$ (log plane),

$$B_1^0 = \exp(-36.426) \exp(+8607/T)\, s^{-0.847}\, m_4^{0.671} \quad (18)$$

for the fourth moment with $r^2 = 0.457$ (log plane), and

$$B_1^0 = \exp(-35.928) \exp(+8545/T)\, s^{-0.831}\, m_5^{0.533} \quad (19)$$

for the fifth moment with $r^2 = 0.433$ (log plane).

BIRTH DISTRIBUTION CORRELATION (METHOD 2)

The correlation of nucleation kinetics through the use of a birth distribution function to account for the appearance of nuclei at the small sizes examined by this study was prompted by the immediate population responses observed in even the larger size particle channels when step changes of stirring rate were made. Thus, the expected delay, if the channels were populated by growth from a lower size, was not observed. The birth distribution function was assumed to be similar in form to a gamma probability function. Thus

$$B(L) = B_2^0 \frac{L^a \exp(-aL/b)}{\Gamma(1+a)\,(b/a)^{1+a}} \quad (20)$$

The gamma distribution was chosen because its value is zero at $L = 0$ and, further, this distribution adequately

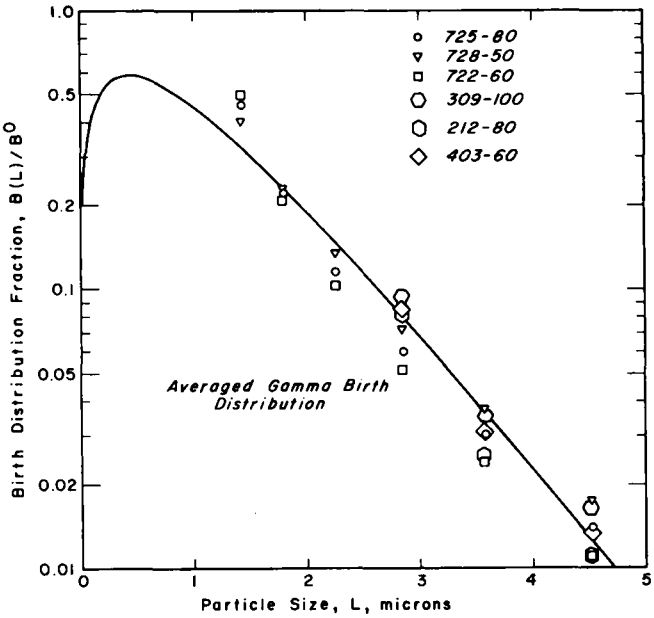

Fig 4. Comparison of normalized $B(L)$ data from six runs with the average gamma birth distribution function.

fits the experimental crystal birth data in the size range studied. It should be pointed out that direct measurements of the birth function were all made at a size larger than the mode size b; measurements in a size range containing the mode will have to be made before the validity of the gamma birth distribution can be verified or disproved. Such measurements are beyond the present technology of particle-size measurement.

Birth function values were calculated according to Equation (8) and fit to Equation (20). Gamma distribution fits could be obtained only when a value for the mode b was specified. Values of b over a wide range were assumed and the $B(L)$ parameters determined for birth data between $L = 1.26$ and 8.0 microns. The best representation of the data was obtained with $b = 0.434$ micron, as given by a maximum value of the correlation coefficient. The values for the wideness parameter a for 114 data sets ranged from 0.481 to 0.612 with an average value of 0.542. Equation (20) was integrated and the resultant total nuclei generation flux B_2^0 determined from each set of constants.

Typical normalized $B(L)$ data are plotted in Figure 4 as well as the curve representing the gamma distribution obtained when $a = 0.542$ and $b = 0.434$ micron. The values of $B(L)$ were fitted to a gamma distribution in log space. The square of the correlation coefficient r^2 ranged in value from 0.957 to 0.990 for the 114 fits performed. Values of B_2^0 ranged from 960 to 44,500 no./cc.-min.

Values of B_2^0 were correlated with Equation (10) in the same manner as described for values of B_1^0. A total of 54 values of B_2^0 representing the same runs and times during each of those runs as used in obtaining correlations (17), (18), and (19) were first evaluated. The common stirring rate of 515 rev./min. for all 24 runs excluded stirring rate as a factor in the correlations. Correlations were made in terms of the third, fourth, and fifth moments of the seed distribution as in the case of the B_1^0 values. The resultant relationships obtained by multiple linear regression of the data are as follows:

$$B_2^0 = \exp(-0.139)\exp(-6556/T)\, s^{0.911} m_3^{1.332} \quad (21)$$

for the third moment with $r^2 = 0.923$ (log plane)

$$B_2^0 = \exp(-3.703)\exp(-6140/T)\, s^{0.705} m_4^{1.104} \quad (22)$$

for the fourth moment with $r^2 = 0.933$ (log plane), and

$$B_2^0 = \exp(-4.507)\exp(-6033/T)\, s^{0.647} m_5^{0.907} \quad (23)$$

for the fifth moment with $r^2 = 0.923$ (log plane).

These correlation coefficients indicate that a more consistent fit is obtained with the B_2^0, rather than the B_1^0, method of data analysis. The effect of supersaturation on nucleation rate predicted by the B_1^0 correlations, namely a decrease in nucleation with an increase in supersaturation, is not consistent with the qualitative observations reported earlier (3). However, this result agrees with the kinetics reported by Randolph and Rajagopal (12) who also defined nucleation rate B_1^0 as the product Gn, but in their case extrapolated to zero size.

A nucleation kinetics model was assumed that had a form similar to Equation (10). However, this model did not stipulate the exact seed distribution moment to be used, that is, the exponents on the total number concentration N_s/V and average size of the seed crystals D_s were allowed to vary independently. Effects of RPM were correlated with a simple exponent of the stirring rate. Thus

$$B_2^0 = k_n \exp(k_1/T)\, s^{k_2} (N_s/V)^{k_3} D_s^{k_4} R_s^{k_5} \quad (24)$$

Equation (24) was fit to 94 values of B_2^0, which data included 40 B_2^0 values evaluated for 9 runs where the stirring rate was either 455 rev./min or 567 rev./min. with the 4-bladed impeller. Again all B_2^0 values were for rhombic seed crystals. The resultant fit of these 94 data points in the above kinetic equation gave the relation

$$B_2^0 = \exp(-42.508)\exp(6067/T)\, s^{0.589} (N_s/V)^{1.182} D_s^{4.471} R_s^{6.137} \quad (25)$$

with $r^2 = 0.930$ (log plane). The ratio $k_4/k_3 = 3.78$ is close to the fourth moment and the k_1, k_2, k_3 values are also near to those values in Equation (22). Therefore, further analysis of the B_2^0 data was based upon the kinetics model of Equation (10) with the fourth moment specified as the correlating variable describing the effect of seed size and magma density.

The final resultant nucleation flux kinetics model that fit the 94 B_2^0 values based upon rhombic seeds gave

$$B_2^0 = \exp(-65.8)\exp(-5440/T)\, s^{0.560} m_4^{1.126} (Re_s)^{5.78} \quad (26)$$

with $r^2 = 0.932$ in the log plane (linear plane $r^2 = 0.930$). Figure 5 shows a comparison of the experimental value of B_2^0 with the B_2^0 values calculated with Equation (26). Variation limits of 30% are indicated by the dashed lines.

Equation (26) was used to calculate 20 other B_2^0 values for comparison with 20 B_2^0 data points obtained with the 3-bladed impeller, polycrystalline seeds, and a distribution of rhombic seeds having a much larger than average length-width ratio. Several estimations were necessary to make the data applicable to Equation (26). The average size of the polycrystalline seeds was approximated, using the mean screen size of the initial seeds and estimation of mean growth rates by comparison to conditions of similar rhombic seeds runs. The average sizes for the abnormally elongated rhombic seed run were calculated from the photographically determined mean size and a growth rate based upon similar runs. The stirring rates used for the 3-bladed impeller were the predetermined 4-bladed impeller

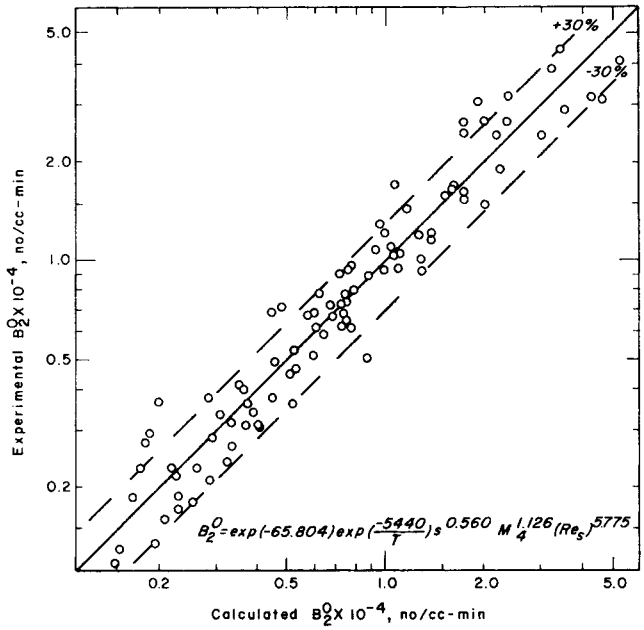

Fig. 5. Comparison of experimental and calculated integral birth fluxes using best 94 point correlation.

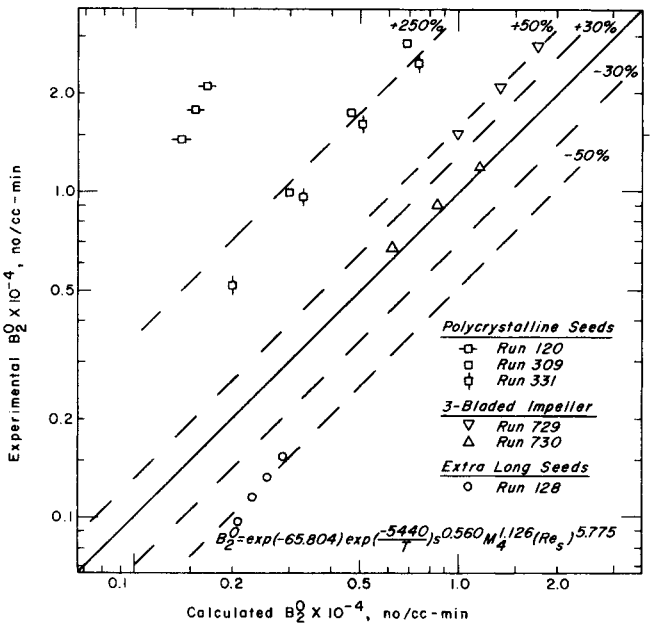

Fig. 6. Examination of the effects of various factors on integral birth flux.

equivalents based upon power input. Figure 6 shows a comparison of the experimental B_2^0 values and the B_2^0 values calculated by using Equation (26) for these twenty data points. Limits of variation of $\pm 30\%$, $\pm 50\%$, and $+250\%$ are indicated by the dashed lines.

Data points for Runs 729 and 730 shown in Figure 6 were obtained using the 3-bladed impeller. All of the experimental B_2^0 values for the 3-bladed impeller are larger than the calculated values from the 4-bladed impeller correlation. The experimental B_2^0 values representing Run 730 performed at 740 rev./min. (the power input equivalent of 515 rev./min. with the 4-bladed impeller) are very close to the values predicted with the 4-bladed impeller correlation. The experimental B_2^0 values for Run 729 performed at 820 rev./min. (equivalent to 567 rev./min. with the 4-bladed impeller) are all approximately 50% greater than the corresponding calculated values. It is apparent that the two sets of B_2^0 data are reasonably well predicted by Equation (26) based upon the 4-bladed equivalent stirring rates; however, the true effect of agitation rate is probably not given uniquely by power input. B_2^0 values for each run tend to parallel the 4-bladed impeller correlation line showing that the functionality of the model is correct. If the trend indicated by the two sets is significant, a correlation using the impeller tip speed and the number of blades may prove a better correlating function than power input itself.

The B_2^0 data shown in Figure 6 for Runs 120, 309, and 331 were obtained using polycrystalline seed crystals. The B_2^0 values calculated for Run 120 using Equation (26) are quite low. The run was of long duration (over 5 hours) compared to the other runs and the experimental values of B_2^0 were based upon population densities obtained approximately 3.5 hours after seeding. The conservative estimation of seed crystal growth rates probably did not account for the actual growth during the extended period of growth experienced by the polycrystalline seeds in this run. Runs 309 and 331 were of much shorter duration and the growth estimates for these runs are more likely to be accurate. In each case the polycrystalline seeds were approximated by an equivalent sphere for size estimation purposes. Experimental B_2^0 values for Runs 309 and 331 are, on the average, two and one-half times larger than the values calculated with Equation (26). This result compares well with the observation reported in (3) that the polycrystalline seed crystals nucleate at a greater rate than rhombic seed crystals.

Values of B_2^0 for Run 128 shown in Figure 6 verify previous qualitative observations (3). The experimental B_2^0 values are one-half those predicted by Equation (26) for the same conditions. Approximately 20% of the crystals in the rhombic seed sample used in Run 128 had a length-width ratio greater than 4. These large crystals tended to roll along the bottom of the crystallizer rather than remain suspended in the agitated slurry. Consequently, these large seed crystals did not contribute as much to the total nucleation rate as their size and mass might indicate. This observation is consistent with the concepts of secondary nucleation by collision breeding mechanisms.

DISCUSSION OF RESULTS

The measured distributions of this study can best be analyzed by considering solutions of the population balance, Equation (4), for various assumed forms of the size-dependent birth and growth functions $B(L)$ and $G(L)$. Examination of some steady state and simple dynamic cases can provide insights into interpreting data such as that illustrated in Figure 1.

Equation (1) predicts that a plot of the log of population density versus particle size should be a straight line. The basic assumptions were steady state operation, constant linear growth rate, no breakage or attrition, clear liquor feed, and perfect mixing. Figure 7a illustrates such a population distribution by the dashed line. When growth rate is size-dependent, increasing with size, a concave upward curved distribution will be obtained. The solid line in Figure 7a shows such a curved population distribution resulting from a size-dependent growth rate expression in which the growth rate increases with increasing particle size. If the growth rate decreases with increasing particle size, the population distribution plot would be concave downward rather than concave upward as shown.

The plots in Figure 7a assume a constant density of

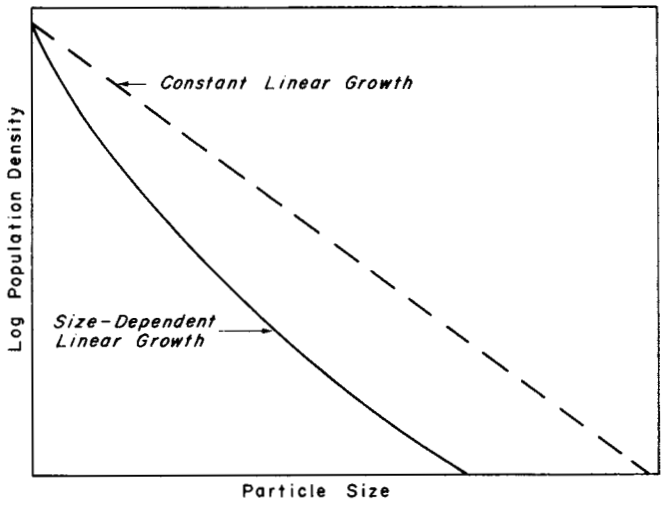

Fig. 7a. Effects of growth rate on population distribution.

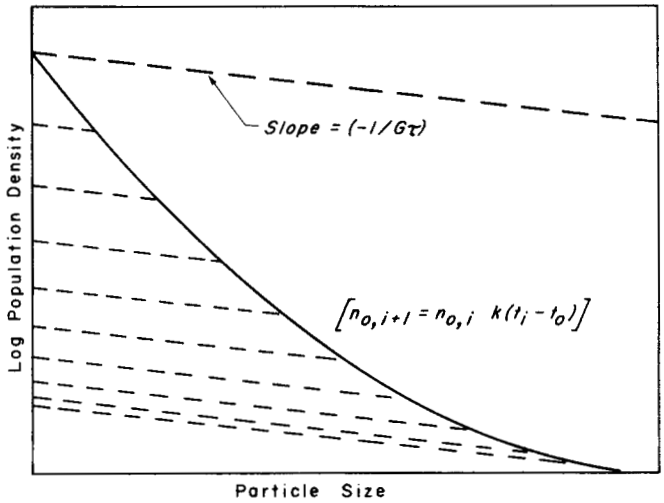

Fig. 7b. Effects of time-dependent nucleation rate on population distribution.

nuclei of negligible size. For the case where nucleation rate increases with time, with a constant growth rate, a population distribution plot such as that shown by the solid line in Figure 7b results. The population density of crystals of zero size formed at any particular time will decay along a particle characteristic having a slope of $-1/G\tau$ shown as the family of parallel dashed lines, with the locus of crystal populations of various ages at any given instant, that is, the current population distribution, as shown by the solid line. Thus, concave-upward curvature can also be induced in a semilog plot of population distribution through an ever-increasing time-dependent nucleation function.

A study of steady state population distributions using the steady state form of Equation (4) was conducted to examine the effects of a birth distribution function upon the overall population distribution. The growth rate was assumed to be constant and a gamma distribution was assumed for the birth function of secondary nuclei $B(L)$. Figure 8 demonstrates the effects on the resulting population distribution of both the average particle size and the width of the assumed gamma-type birth distribution. In all cases the integral of the birth distribution function equaled the value of B^0 used in the population distribution of the MSMPR case; this latter distribution appears as the straight dashed line in Figure 8.

Figure 8a shows the effect of increasing average size of the gamma-type birth distribution on the population distribution. The average sizes assumed were 0.5, 1.0, and 2.0 microns. In all three cases the coefficient of variation of the birth distribution was 0.20. The three curves show that as size increases to where the size ranges are populated by growth convection rather than birth, the population distribution becomes a straight line parallel and above the idealized MSMPR distribution predicted by Equation (1). Each curve is shifted to the right according to the magnitude of the mean size of the birth distribution.

Figure 8b illustrates the effect of varying the coefficient of variation of the birth distribution at a mean size of 2.0 microns. As the coefficient of variation decreases given by the innermost curves, the distribution rises steeply and approaches a straight line parallel to the MSMPR dashed line but shifted to the right by 2.0 microns on the size axis. All of the curves shown in Figure 8 are concave downward and approach a straight population decay line as an asymptotic limit. In no case, with size-independent growth rate, can a steady state birth distribution cause the population distribution to overshoot the final path of the straight decay section. Thus, a birth distribution by itself cannot induce a concave upward population distribution as exhibited by the data of this study (3).

Equation (4) was also solved to study the steady state population distribution resulting from a birth distribution

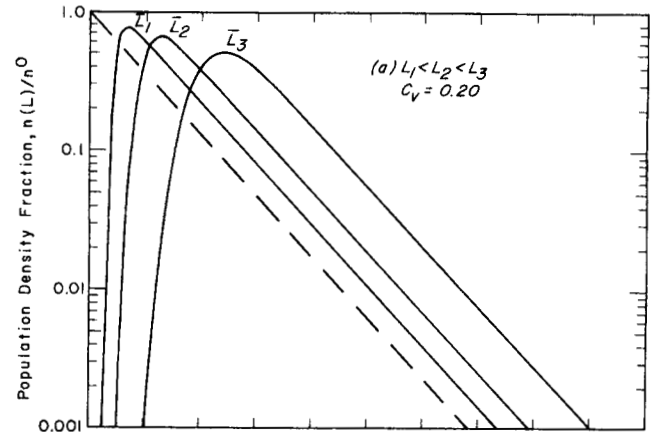

Fig. 8a. Effect of gamma birth distribution functions on population distribution. Effect of mean size of the distribution.

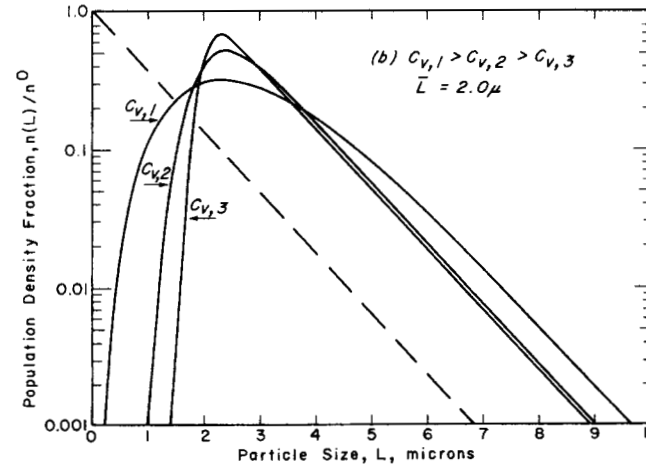

Fig. 8b. Effect of gamma birth distribution functions on population distribution. Effect of coefficient of variation.

function and a size-dependent growth function. These calculations combine the effects shown in Figures 7a and 8 and produced the desired concave-upward population distribution. No attempt was made to rigorously model the experimental data due to the impossibility of a priori distinguishing between the effects produced by different $B(L)$ and $G(L)$ functions.

GROWTH RATE KINETICS

The most surprising and significant result of the present study was observation of the extreme size-dependency of growth rates of the fine crystal distribution as illustrated in Figure 2. The low growth rates of secondary nuclei and the erratic and different (relative to seed crystals) dependency of these growth rates on supersaturation exert a profound influence on the net apparent nucleation kinetics observed in MSMPR studies. This phenomenon is illustrated in the following discussion.

The apparent dependency on supersaturation of the fine-crystal growth rates were of the form $s^{0.99}$ ($r^2 = 0.425$) while the seed-crystal growth rates varied as $s^{1.93}$ ($r^2 = 0.954$). Only a small fraction of the secondary nuclei observed would grow to populate the macro-sized product distribution observed by screen analysis; their low growth rates indicate that greater than 99 in 100 secondary nuclei would be washed out of the system before growing to an appreciable size affecting the product distribution. The exponential decay rate of population for any size is proportional to $1/G\tau$ and would thus be greatly different for the fine-crystal and product-sized distributions. Further, changes in the mean retention time τ in MSMPR studies are used to bring about changes in the supersaturation driving forces s and growth rates G. Thus, different relative changes in washout rate of the fine-crystals and product-sized crystals would be brought about by a given change in τ due to the differing changes in growth at the new supersaturation level. The number of net surviving nuclei (apparent MSMPR nuclei) are critically dependent on the degree of exponential decay of the slow-growing secondary nuclei. Thus, positive, negative, or zero kinetic orders of apparent nucleation rate with supersaturation might be observed, depending on the differing supersaturation dependency of growth rates for the nuclei and product sizes.

To illustrate, the true dependency of secondary nucleation (assuming the B_2^0 analysis is an adequate representation of secondary nucleation) for the K_2SO_4 system is of the order of $s^{0.6}$, yet Rosen and Hulburt (*15*) and Genck and Larson (*5*) report essentially zero-order supersaturation dependency from analysis of MSMPR data. A negative supersaturation dependency of nucleation is observed in this study and by Randolph and Rajagopal (*12*) when secondary nucleation was interpreted (incorrectly) by the particle flux technique. This apparent anomaly is explained as follows. Assume an MSMPR crystallizer (K_2SO_4) operating at a given retention time τ. Throughput is then increased (smaller τ) forcing supersaturation to a higher level. The growth rate of secondary nuclei increases approximately as s while the product crystals increases as s^2. The net effect is a higher washout rate of nuclei (relative to product) essentially cancelling the increased secondary nucleation ($\sim s^{0.6}$) and yielding zero-order response of net apparent nucleation rate with supersaturation.

This phenomenon also explains the observation that retention time (not a state variable) must often be included in MSMPR kinetic correlations to give an adequate correlation of the data. Thus, the number of surviving nuclei depends explicitly on τ as well as implicitly on $s(\tau)$, where changes in s were brought about by changes in τ. True nucleation rate should only depend on the state variables characterizing the magma at any instant.

CSD FROM NUCLEATION CORRELATIONS

The limiting assumption that growth rates were negligible in the fine-crystal size range was necessary in evaluating B_2^0 as no growth rate model was known or could be independently determined. It is apparent that growth is not identically zero as some of the secondary nuclei must surely survive to populate the larger size ranges. Values of B_1^0 and B_2^0 are approximations of the nucleation rate, which approximations are made necessary by the impossibility of determining simultaneously the unknown functions $B(L)$ and $G(L)$. The good correlation coefficients of B_2^0 data indicate that this is the better limiting assumption.

If the B_2^0 correlation of this study is evaluated at conditions comprising normal crystallizer operation the predicted nucleation rate is approximately two orders of magnitude greater than that observed from MSMPR data. Either these excess secondary nuclei are washed out during their slow-growth period or the kinetic measurements of this study are grossly in error. (The latter case was certainly not ruled out, but exhaustive checks of background noise, mixed removal at the size range measured (*3*), and instrument calibration revealed that the only possibility for data errors of this magnitude would be if counts in the smaller size ranges, giving negligible background noise when the crystallizer was unseeded, suddenly produced particle counts in error by two orders of magnitude as secondary nuclei appeared in the crystallizer discharge.)

The B_2^0 kinetics of this study were evaluated at the MSMPR conditions of Genck (*5*) and the amount of surviving nuclei estimated using the (maximum) fine-crystal growth rate correlation, Equations (12) and (14). The values of k and G_∞ were taken from a typical run performed in this study (Run 212, 120 minutes); G_∞ was scaled to the supersaturation of Genck's experiment according to the first-order supersaturation effect predicted by Equation (14). The effect of size-dependent growth on the washout rate of nuclei being generated at an original rate B_2^0 was represented by an exponential decay term $\exp(-\tau_D/\tau)$, where τ_D is the growth "dead time" and τ is the crystallizer retention time. The growth dead time was calculated using the fine-crystal growth correlation evaluated at Genck's conditions and was arbitrarily assumed to be the time it took for a nuclei particle to grow from the mode of the gamma birth distribution function, 0.434 micron, to an upper limit of 9 microns (where the drastic size-dependency of growth rate is greatly diminished and the birth function becomes negligible). Thus, the corrected nucleation rate B_{2c}^0 was defined as

$$B_{2c}^0 = B_2^0 \exp(-\tau_D/\tau) \tag{27}$$

where the growth dead time is given as

$$\tau_D = \int_{0.434}^{9.0} \frac{dL}{G(L)} = \int_{0.434}^{9.0} \left(\frac{1}{G_\infty}\right)\left(\frac{s}{s_G}\right) \exp(-k/\sqrt{L})\, dL \tag{28}$$

The supersaturation measured by Genck (*5*) in his experiment was 3.1 g/l, M_T was measured as 0.0142 g/cc and

the particle retention time was 15 minutes. The nuclei growth dead time, at the experimental conditions reported by Genck, was determined to be 168 minutes. This value is sensitive to the lower size limit (0.434μ) but not to the upper limit (9μ). The value of 0.434μ is the estimated mode size and represents a typical secondary nucleus.

The 94 B_2^0 data sets for the rhombic seed runs that were correlated by Equation (26) were reanalyzed using the solids concentration, M_T (with units of g/cc for this case), rather than the fourth seed moment. This correlation was then evaluated at Genck's operating temperature of 30°C and the median stirring rate used in this study of 515 rev./min. The resultant value of B_{2c}^0 obtained in the aforementioned manner was 208 no./cc.-min. This value was divided by Genck's reported value of growth rate at zero size to give a value for the nuclei density n_0 of 54.9 no./cc.-micron. Genck reported an n_0 value of 38.9 no./cc.-micron obtained by extrapolation of his size distribution data. Thus, the nucleation rates of this study appear reasonable, when extrapolated to MSMPR conditions, if these rates are corrected for the washout occurring during the initial period of slow growth. All size channels in this study, even those greater than 9 microns, were certainly populated in less than 168 minutes; however, there was evidence of direct birth in each size channel measured.

It thus appears that the majority of secondary nuclei, created in size at the lower end of the size range, are largely ineffective in populating the product-size ranges. Certainly, without an accurate and independently measured growth function $G(L)$, there is no way to quantitatively use the secondary nucleation birth kinetics B_2^0, say as correlated by Equation (26), in rigorous CSD calculations.

MSMPR-derived kinetic correlations, although representing only net apparent nucleation rates, remain the most useful technique for CSD simulation in systems not far removed from MSMPR operation. True secondary nucleation kinetics can only be defined from $n(L)$ measurements when the correct form of the size-dependent functions $G(L)$ and $B(L)$ can be independently measured.

SUMMARY AND CONCLUSIONS

1. Population density data for the potassium sulfate system in the 1.3-26 micron size range were analyzed by two techniques using two limiting assumptions to define secondary nucleation rates in the system. The limiting assumptions, that nucleation occurs at some lower size and all size ranges are populated by particle growth or that nucleation is predominately by direct birth at a size, gave comparable values for nucleation rate, but values calculated by the latter technique correlated better with operating conditions. Both calculational techniques gave nucleation rates two orders of magnitude in excess of MSMPR data.

2. Secondary nucleation power-law kinetic models of the type used to correlate MSMPR nucleation rates were adequate to correlate these data; the best correlation of the data (rhombic seed crystals) of this study was

$$B^0 = \exp(-65.8)\exp(-5440/T)\, s^{0.56}\, m_4^{1.126}(Re_s)^{5.78}$$

3. Growth rates of crystals in the 1.3-26 micron size range are markedly size-dependent, decreasing with decreasing size.

4. The very small growth rates of secondary nuclei indicate that most are washed out of the system before growing to populate the size ranges observed on typical MSMPR studies. Correction for washout gives net nucleation rates comparable to MSMPR values.

5. For the system studied, the supersaturation dependence of growth rates for secondary nuclei and product-sized crystals is different. This phenomenon affects the washout survival rate of fine-crystals relative to product-crystals and explains the anomalous nucleation-supersaturation dependence reported for potassium sulfate from MSMPR studies.

6. The quantitative definition and use of secondary nucleation kinetics as developed in this study must await more refined population measurements at lower sizes as well as independent measurement of either the particle birth function $B(L)$ or the crystal growth rate $G(L)$.

ACKNOWLEDGMENT

The authors gratefully acknowledge the support of the National Science Foundation through grant GK-10551.

NOTATION

B^0 = net apparent nucleation rate, no./cc.-min.
B_1^0 = nucleation rate based on particle flux method, no./cc.-min.
B_2^0 = nucleation rate based on integral of birth distribution, no./cc.-min.
$B(L)$ = secondary nuclei birth distribution function, no./cc.-min.-μ
$D(L)$ = crystal breakage function, no./cc.-min.-μ
D_s = average diameter of seed crystals, μ
G = linear crystal growth rate, μ/min.
G_p = growth rate of seed crystals, μ/min.
G_∞ = parameter in fine-crystal growth function, equal to extrapolated macro-crystal growth rate, μ/min.
k_g = rate constant in growth rate expression
k_N = rate constant in nucleation kinetics expression
L = crystal size, μ
M_T = slurry solids concentration, g./cc.
m_j = j'th moment about zero of population distribution, $\approx D_s^j N_s$ for narrow seed-crystal distribution
$n(L)$ = crystal population density. no./cc.-μ
N_s = seed-crystal population, no./cc.
$N(L)$ = crystal population flux, equal to $n(L)G(L)$, no./cc.-min.
R_s = stirrer RPM
s = solute supersaturation, gm./l.
T = absolute temperature, °K.
t = time, min.
V = crystallizer volume, cc.
τ = mean crystallizer retention time, V/Q, min.

LITERATURE CITED

1. Bransom, S. H., W. J. Dunning, and B. Millard, *Disc. Faraday Soc.*, **5**, 83 (1949).
2. Cise, M. D., "Crystal Growth and Nucleation Kinetics of the Potassium Sulfate System in a Continuous-Flow, Seeded Crystallizer," Ph.D thesis, Univ. Arizona, Tucson (1971).
3. Cise, M. D., and A. D. Randolph, *Chem. Eng. Progr. Symp. Ser., No. 121*, **68**, 42 (1972).
4. Clontz, N. A., and W. L. McCabe, *Chem. Eng. Progr. Symp. Ser. No. 110*, **67**, 6 (1971).
5. Genck, W. J., unpublished Ph.D. thesis, Iowa State Univ., Ames (1970).
6. Ishii, T., *Bull. Tokyo Inst. Tech. No. 67* (1965).

7. Larson, M. A., and A. D. Randolph, *Chem. Eng. Progr. Ser. No. 95*, **65**, 1 (1969).
8. Mason, R. E. A., and R. F. Strickland-Constable, *Trans. Faraday Soc.*, **62**, 455 (1966).
9. Mullin, J. W., and C. Gaska, *Can. J. Chem. Eng.*, **47**, 483 (1969).
10. Randolph, A. D., *ibid.*, **42**, 280 (1964).
11. ———., *AIChE J.*, **11**, 424 (1965).
12. ———., and K. Rajagopal, *Ind. Eng. Chem. Fundamentals*, **9**, 165 (1970).
13. Randolph, A. D., *Chem. Eng.*, **77**, 80 (1970).
14. Rosen, H. N., and H. M. Hulburt, *Chem. Eng. Progr. Symp. Ser. No. 110*, **67**, 27 (1971).
15. *Ibid.*, 18.

Manuscript received October 1, 1971; revision received March 3, 1972; paper accepted March 30, 1972.

Kinetics and Mechanism of the Epoxidation of Unsaturated Fatty Acids

A study was made of the epoxidation of octadecenoic acids with peroxybenzoic acid in benzene. Activation energies, frequency factors, enthalpies of activation, entropies of activation, and free energies of activation were obtained for the following fatty acids: *cis*-9-octadecenoic acid (oleic), *trans*-9-octadecenoic acid (elaidic), 12-hydroxy-*cis*-9-octadecenoic acid (ricinoleic), 12-hydroxy-*trans*-9-octadecenoic acid (ricinelaidic), *cis*-11-octadecenoic acid (vaccenic), and *cis*-6-octadecenoic acid (petroselinic). It was observed that the reaction rate was adversely affected by the proximity of the carboxyl group, that is, the closer the carboxyl to the reaction site the lower the rate. A shift from a *trans* to a *cis* configuration results in an approximate 50% increase in reaction rate with a corresponding decrease in free energy of activation of 260 cal/mol. The effects of isomerism and the replacement of substituent groups on the reaction rate were generally additive. A mechanism for the peroxydation of octadecenoic acids is proposed.

M. E. ABRAHAM
and R. F. BENENATI
Polytechnic Institute of Brooklyn
Brooklyn, New York

SCOPE

Epoxidation is a controlled reaction of an unsaturated compound with a relatively mild oxidizing agent to give an epoxy (oxirane) compound. At the present time, the peracid most used commercially in epoxidation is peracetic acid. It is readily prepared from hydrogen peroxide and glacial acetic acid in the presence of a strong acid catalyst such as sulfuric acid.

While peracetic acid is the compound of choice commercially, it is difficult to use in making the type of fundamental studies reported here because it is unstable in its pure form. Its tendency to decompose makes analysis difficult. One cannot be sure whether the disappearance of the peracid in the course of the study is due to epoxidation or simple decomposition. As a result, due to its greater stability perbenzoic acid was chosen for this study. Perbenzoic acid has the additional advantages that it can be obtained as a pure compound with a minimum of hazard and tends to react more completely. Consequently, kinetic data and experiments undertaken to develop mechanistic information are much more accurate.

The empirical observations of numerous workers concerned with the epoxidation reaction since its discovery at the turn of the century have pointed out that under similar experimental conditions the rate of reaction of olefins with organic peracids is a function of the structure of the unsaturated compounds. Over the years many attempts were made to explain this behavior. D. Swern in 1947, 1948, and 1953 proposed several theories. In 1953 he suggested a mechanism in which the transition state would be similar to the so-called "pi complexes." In 1951 Badger proposed a molecular addition to one of the carbons adjacent to the double bond. In 1955 Lynch and Pausacker said the olefinic bond itself was attacked. Edward and Cohen in 1960 suggested an ionic or free radical mechanism for the decomposition of perbenzoic acid depending on media; while in 1962 and 1963 Tokumaru et al., proposed a free radical mechanism. Thus, the

Correspondence concerning this paper should be addressed to M. E. Abraham at R. B. MacMullin Associates, Niagara Falls, New York 14303.